Evaluating the adequateness of kinematic-wave routing for flood forecasting in midstream channel reaches of Taiwan

Kwan Tun Lee and Pin-Chun Huang

ABSTRACT

An efficient flood forecasting system can provide useful advance information for evacuating people in order to mitigate potential disaster. In Taiwan, a kinematic-wave approximation of the full dynamic-wave equations is usually adopted in upstream and midstream steep channel reaches to avoid numerical instability when performing a flood forecast. Although the kinematic-wave approximation does provide a convenient simulation, questions arise with respect to its applicability and accuracy. In this study, numerical algorithms were developed to investigate the deviations of the hydrograph peak discharge and the time to peak discharge using the dynamic- and kinematic-wave methods. A series of numerical experiments were performed to investigate the hydrograph deviations using these two methods. Numerical results show that the flood-peak attenuation generated using the dynamic-wave method is more significant than that using the kinematic-wave approximation, and also that flow hydrographs generated using the dynamic-wave method always precede those using the kinematic-wave approximation. Regression results demonstrate that channel slope and roughness dominate the flood hydrograph attenuation and translation. Nevertheless, hydrograph deviations between these two methods were found to be small for a channel slope larger than 0.001, which can therefore be recognized as a criterion for ensuring the precision of the kinematic-wave approximation.

Key words | dynamic-wave routing, flood forecasting, kinematic-wave routing

Kwan Tun Lee (corresponding author)
Pin-Chun Huang
Department of River & Harbor Engineering,
National Taiwan Ocean University,
Keelung,
Taiwan 202,
Chinese Taiwan
E-mail: *ktlee@ntou.edu.tw*

Kwan Tun Lee
Taiwan Typhoon and Flood Research Institute,
Taichung,
Taiwan 407,
Chinese Taiwan

INTRODUCTION

The average annual rainfall in Taiwan is about 2,500 mm. Hydrological records show that high rainfall intensity caused by typhoons and thunderstorms occurs mainly between May and October. There are an average of 3.6 typhoons per year that cause severe flooding and consequent loss of life and property. Taking into consideration the limited protection provided by engineering structures, an efficient flood warning system may be able to provide authorities useful advance information for evacuating people to mitigate casualties in the event of disaster.

The advent of high-speed computing permits the simulation of temporal and spatial flow on overland areas and in channels. The full Saint-Venant equations are usually adopted to perform the flood routing using a particular numerical method, denoted as the dynamic-wave method (Fread 1973; Price 1974; Cunge *et al.* 1980; Fread 1985; Jin & Fread 1997; Ying *et al.* 2004). In performing dynamic-wave routing, the flood wave translation is controlled by resistance, gravity, pressure, and inertial forces. When inertial forces are neglected, the flood simulation is denoted as a non-inertia wave approximation (Price 1973; Ponce *et al.* 1978; Akan & Yen 1981; Cappelaere 1997; Yen & Tsai 2001; Huang & Lee 2009), and the component of pressure force due to the difference between the bed slope and the water-depth gradient in the momentum equation can be further omitted to create the kinematic-wave approximation,

which is usually adopted for channel-flow routing in steep channels or in simulating overland flow in upstream watersheds (Lighthill & Whitham 1955; Iwagaki 1955; Henderson & Wooding 1964; Wooding 1965; Cundy & Tento 1985; Lee & Yen 1997; Jaber & Mohtar 2003; Tseng 2010).

In performing an unsteady-flow simulation, the Preissmann scheme (Preissmann 1961), an efficient implicit finite-difference method, is widely used to generate approximate solutions of the dynamic wave. The scheme is unconditionally stable for subcritical flow and possesses considerable flexibility in the selection of spatial increments and time steps. However, the stability of the Preissmann scheme is not maintained in transcritical flow conditions. Using Fourier stability analysis, Samuels & Skeels (1990) showed that the Preissmann scheme must be forward weighted, $\theta \geq 0.5$ and that the Vedernikov number should be less than unity. Meselhe & Holly (1997) further reported that the Preissmann scheme is marginally stable if critical flow is encountered. Although artificial viscosity can be used to offer some damping, it may compromise computational efficiency. Hence, the unconditional stability of the Preissmann scheme is invalidated for critical flows. In practical flood routing, the conversion of subcritical to supercritical can be encountered as the channel bed gradually becomes steeper from the estuary to the upstream channel head. Consequently, some upstream channel reaches may require the simulation of transcritical flow. Although the kinematic-wave approximation seems to be a good alternative, its applicability and accuracy may be questioned.

From a mathematical standpoint, the kinematic-wave approximation leads to a considerable simplification of the momentum equation through the assumption of uniform flow. The kinematic-wave cannot describe authentic physical diffusion due to the assumed omission of inertial forces and pressure (Ponce 1991); but solutions of certain forms of the finite-difference scheme for the kinematic-wave are shown to possess intrinsic amounts of numerical diffusion which can modify the peak and shape of the hydrograph (Abbott 1976). Cunge (1969) extended the Muskingum method to time variable parameters and recognized that the original Muskingum approach could be viewed as a first-order kinematic approximation of a diffusion-wave model;

however, the Muskingum–Cunge method suffers from a loss of mass, especially for mild bed slope (Ponce & Yevjevich 1978; Tang et al. 1999). More recently, a modified version of the Muskingum–Cunge method has been developed to preserve mass conservation in performing flood routing (Todini 2007; Price 2009).

Since the physical and numerical diffusion are both presented in the dynamic-wave algorithm, an appreciable difference in the predicted flow hydrographs may emerge between the dynamic- and kinematic-wave routing methods under specified conditions. Moreover, in addition to physical diffusion, two more accelerating factors, inertial forces and pressure force, included in the dynamic-wave method can result in a difference in flood-wave propagation when compared to results obtained using the kinematic-wave approximation. This study is designed to investigate the differences between flood hydrographs generated using these two methods. First, numerical algorithms for these two methods were developed. Dimensional analysis was then applied to obtain the independent variables to be used as control factors in performing a series of numerical experiments. As shown in Figure 1, deviations of hydrograph peak discharge (ΔQ_p) and time to peak discharge (ΔT_p) using these two flood-routing methods were investigated in detail. The results of the numerical experiments presented herein are intended to provide information for engineers in determining adequate hydrodynamic routing methods for practical flood forecasting in channel reaches with different geometries.
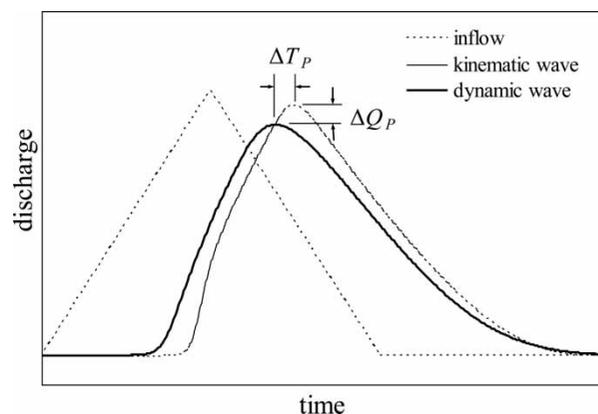

Figure 1 | Schematic of hydrographs routed by using dynamic- and kinematic-wave methods.

DYNAMIC- AND KINEMATIC-WAVE ROUTING METHODS FOR FLOOD FORECASTING

The continuity and momentum equations for one-dimensional unsteady open-channel flow, also known as the Saint-Venant equations, are:

$$\frac{\partial A}{\partial t} + \frac{\partial Q}{\partial x} = q_l \tag{1}$$

$$\frac{\partial Q}{\partial t} + \frac{\partial(\beta QV)}{\partial x} + gA\frac{\partial y}{\partial x} = gA(S_o - S_f) + \beta q_l V_x \tag{2}$$

in which A = cross-sectional area of flow; Q = flow discharge; q_l = lateral flow; β = momentum coefficient; V = flow velocity; g = gravity acceleration; y = water depth; S_o = channel slope; S_f = friction slope; t = time; and x = distance along the channel. Neglecting the influence of lateral flow, the non-conservation form of the momentum equation for a unit channel width is:

$$S_f = S_o - \frac{\partial y}{\partial x} - \frac{V}{g}\frac{\partial V}{\partial x} - \frac{1}{g}\frac{\partial V}{\partial t} \tag{3}$$

This equation represents the flood transport in dynamic-wave form, sequentially taking into account the force terms shown on the right-hand side of the equal sign, including gravity, pressure, convective inertia, and local inertia forces. When the inertial forces are omitted, the equation describes the non-inertia wave approximation, and it is known as the kinematic-wave approximation when both the inertial forces and the pressure force due to the difference between the bed slope and water-depth gradient are omitted. Consequently, the simplified momentum equation for the kinematic-wave approximation is:

$$S_f = S_o \tag{4}$$

The kinematic wave method has been shown to provide good simulation results for runoff analysis in steep overland areas and steep channels.

Dynamic-wave algorithm

Equations (1) and (2) are nonlinear hyperbolic partial differential equations for which analytical solutions are unavailable. Numerical solutions can be obtained if appropriate initial and boundary conditions are properly prescribed. In this study, a four-point Preissmann implicit finite-difference approximation was used, which can be expressed as

$$\frac{\partial f}{\partial x} = \frac{1}{\Delta x}\left[\theta(f_{i+1}^{j+1} - f_i^{j+1}) + (1-\theta)(f_{i+1}^j - f_i^j)\right] \tag{5}$$

$$\frac{\partial f}{\partial t} = \frac{1}{2\Delta t}\left[(f_{i+1}^{j+1} - f_{i+1}^j) + (f_i^{j+1} - f_i^j)\right] \tag{6}$$

and

$$f(x, t) = \theta(f_{i+1}^{j+1} + f_i^{j+1}) + (1-\theta)(f_{i+1}^j + f_i^j) \tag{7}$$

in which $f = a$ variable represents discharge or water depth; i = space coordinate; j = time coordinate; θ = weighting coefficient. In the discretization processes, two adjacent channel cross-sections can be organized to provide two equations with four unknown variables containing discharge and water depth at the advance time level. On the other hand, because of the non-linearity, the solution needs to be obtained using an iterative procedure. A Taylor expansion for solving the nonlinear system used herein can convert the original differential equations to linear forms.

In applying an implicit-difference scheme, the unknown values are derived simultaneously; inefficiency can occur when solving a large matrix with respect to a large number of channel cross-sections. A double-sweep method was adopted to improve computational efficiency. By appropriate elimination and substitution in the matrix, unknown values at each cross-section along the stream can be obtained in sequence starting from the upstream section and moving to the downstream outlet of the channel with given boundary conditions.

Kinematic wave algorithm

The simplest hydrodynamic model therefore is the kinematic-wave approximation. The simplified momentum equation shown in Equation (4) can be transformed into a

nonlinear relationship between flow area and discharge as:

$$A = \alpha_c Q^m \tag{8}$$

where α_c and m are constants. The constant α_c can be recognized as $(nP^{2/3}/\sqrt{S})^{3/5}$ and m as 3/5 from Manning's equation, in which n is the roughness coefficient and P is the wetted perimeter. Differentiating Equation (8) and substituting into Equation (1) gives:

$$\alpha_c m Q^{m-1} \frac{\partial Q}{\partial t} + \frac{\partial Q}{\partial x} = q_l \tag{9}$$

A linear explicit backward-difference method can be used to discretize Equation (9) to obtain the unknown Q_{i+1}^{j+1} as (Chow *et al.* 1988):

$$Q_{i+1}^{j+1} = \frac{(\Delta t/\Delta x)Q_i^{j+1} + \alpha_c m Q_{i+1}^j [(Q_{i+1}^j + Q_i^{j+1}/2)]^{m-1} + \Delta t q_l^{j+1}}{(\Delta t/\Delta x) + \alpha_c m [(Q_{i+1}^j + Q_i^{j+1}/2)]^{m-1}} \tag{10}$$

where Δx is the spatial increment, and Δt is the temporal increment. This explicit numerical scheme is necessary to satisfy the Courant–Friedrichs–Lewy criterion (Courant *et al.* 1967) which restricts the ratio of spatial and temporal increments in the calculation.

Practical approaches for flood forecasting in Taiwan

Taiwan is located between Japan and the Philippines in the Western Pacific and has a total area of 36,000 km². The island is 400 km long with a maximum width of 140 km, and the Central Mountain ranges in the middle of the island. The mountainous area with elevations higher than 1,000 m occupies 32% of the island, which results in steep upstream and midstream channel reaches with rapid stream flow; but the steep channels adjust abruptly to mild slopes within a short distance and then flow into the ocean. Consequently, in developing a flood forecasting system, the dynamic-wave method is adopted to account for the tidal effect in the downstream mild channel reaches, and the kinematic-wave approximation is usually applied to the steep midstream channel reaches to avoid numerical instability in performing real-time flood forecasting.

Hence, the question arises as to the appropriate location of a demarcation point to connect these two flood-routing methods in a river from downstream to upstream. This demarcation point should vary with different channel geometries, bed slopes, and flow conditions.

In this study, the Chung-Kang River, located in northern Taiwan, was used as an example to highlight the dilemma of defining the demarcation point to link the dynamic-wave and the kinematic-wave routing algorithms. The watershed area of Chung-Kang River is 448 km² with an average slope of 0.28. The main stream length is 57 km with a channel width of 300 m at the estuary narrowing to 120 m at 30 km upstream from the estuary. Data for 89 channel cross-sections were collected for the unsteady channel-flow routing, which explicitly showed a very mild slope channel in the downstream reach near the estuary, turning to a steep slope of more than 0.005 m m^{-1} within only a distance of 8.8 km. The topography of the Chung-Kang River is basically similar to the general channel-bed profiles observed in Taiwan.

In performing the numerical tests, different flow discharges were assigned. As shown in Figure 2, for a 100-yr return period the discharge is 8,694 m³ s^{-1}; to avoid numerical instability, the dynamic-wave routing algorithm can only be applied to channel reaches from the estuary to a point 11,564 m upstream (point X_1), while the kinematic-wave routing algorithm is used for flood routing in the upstream channel above point X_1. Nevertheless, the demarcation shifts from X_1 to X_2 (16,623 m upstream from the estuary) when using the 10-yr return period discharge of 3,059 m³ s^{-1} for channel-flow routing. For a discharge of 987 m³ s^{-1}, corresponding to a 2-yr return period, the point separating the dynamic-wave and kinematic-wave methods moves to X_3 (25,654 m upstream from the estuary). In considering public safety during high return-period floods, point X_1 should be chosen as the demarcation to separate the two routing methods in order to meet the stringent requirements of numerical stability in performing real-time flood forecasting. It is therefore worth investigating whether the kinematic-wave approximation can adequately describe the flood wave propagation in the channel reaches between X_1 and X_3. Consequently, further numerical experiments should be conducted to quantify the deviation in the hydrograph generated using these two flood routing methods.
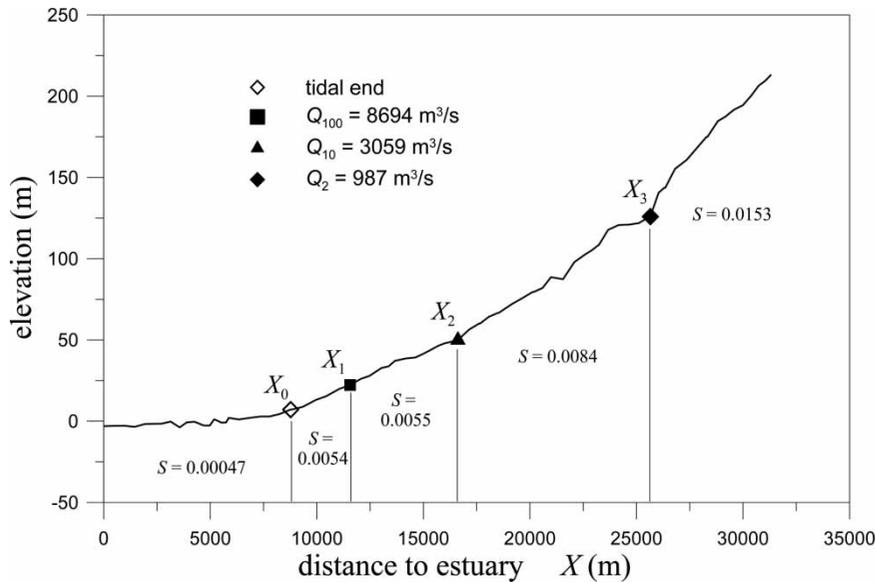
Figure 2 | Numerical instability points of dynamic-wave routing for the Chung-Kang River corresponding to different flow discharges.

VARIABLE DETERMINATION FOR NUMERICAL EXPERIMENTS

The accuracy of a flood-wave simulation using the kinematic-wave approximation should be examined because two acceleration terms have been omitted in the momentum equation of the dynamic-wave method. Consequently, the applicability of the kinematic-wave method under various flow and channel geometry conditions needs to be investigated. As shown in Figure 1, if a triangular hydrograph is adopted as the upstream inflow boundary, it is easy to explore the differences in peak discharge and time to peak discharge between the downstream outflow hydrographs generated using the dynamic- and kinematic-wave methods. The investigation for the deviations of peak discharge and time to peak discharge aims at evaluating the effects of omitting the physical diffusion and delay of flood-wave propagation when using the kinematic-wave approximation. Two dimensionless parameters are used to evaluate the differences of the hydrograph with respect to peak discharge and time to peak discharge, which can be expressed as:

$$DQ_p = \frac{(Q_p)_K - (Q_p)_D}{(Q_p)_D} \tag{11}$$

$$DT_p = \frac{(T_p)_K - (T_p)_D}{(T_p)_D} \tag{12}$$

where DQ_p = peak-discharge deviation; $(Q_P)_K$ = outflow peak discharge by using kinematic-wave method; $(Q_P)_D$ = outflow peak discharge by using dynamic-wave method; DT_p = time to peak discharge deviation; $(T_P)_K$ = time to peak discharge using the kinematic-wave method; $(T_P)_D$ = time to peak discharge using the dynamic-wave method.

The deviations are expected to be influenced by the flow and the channel geometry. If a rectangular channel shape is applied to simplify the problem, factors affecting the peak discharge deviation and time to peak discharge deviation can be expressed as:

$$DQ_P, DT_P = f(S, n, B, g, V_{IP}, y_{IP}, \rho, \mu, L) \tag{13}$$

in which S = channel slope; n = channel roughness; B = channel width; g = gravity acceleration; V_{IP} = velocity of the upstream inflow hydrograph at peak, y_{IP} = depth of the upstream inflow hydrograph at peak; ρ = fluid density; μ = fluid viscosity; L = channel length. By selecting V_{IP}, y_{IP} and ρ as redundant variables, the independent variables

can be rearranged into the following dimensionless form:

$$\mathrm{DQ_p, DT_p} = f\left(S, n, \frac{B}{y_{IP}}, \frac{V_{IP}}{\sqrt{g y_{IP}}}, \frac{\rho y_{IP} V_{IP}}{\mu}, \frac{L}{y_{IP}}\right) \qquad (14)$$

The influences of fluid viscosity in rough turbulent open-channel flow can be ignored; hence, the Reynolds number (the fifth term) can be omitted from Equation (14). For a specified channel reach, the last term in Equation (14) can also be omitted. Moreover, because the main consideration of this work is the attenuation of flood peak discharge, the flow velocity in the fourth term of Equation (14) should be converted to flow discharge. Consequently, the revised form of the dimensional analysis can be expressed as:

$$\mathrm{DQ_p, DT_p} = f\left(S, n, \frac{B}{y_{IP}}, \frac{Q_{IP}}{g^{1/2} B y_{IP}^{3/2}}\right) \qquad (15)$$

in which, Q_{IP} = peak discharge of the upstream inflow hydrograph.

Based on the results obtained from the dimensional analysis, the deviations of hydrographs generated using the dynamic- and kinematic-wave methods depend on the channel slope, channel roughness, ratio of channel width to water depth, and Froude number. The parameters can then be examined through a series of numerical tests to identify the importance of the independent variables on hydrograph deviation when using different flood-routing methods.

RESULTS AND DISCUSSION

Various values of the independent variables shown in Equation (15) were assigned to investigate the deviation of the downstream outflow hydrographs using different methods. The ranges of the assigned values for the independent variables were selected according to the flow and channel geometry conditions collected from the downstream and midstream channel reaches of many rivers in Taiwan. A rectangular channel with different widths was adopted in the current study to simplify the problem. The design of the numerical experiments was based on the geomorphologic and hydrological conditions of Taiwan.

Adopting a triangular hydrograph as the upstream inflow boundary makes it simple in exploring the differences of the downstream outflow hydrographs generated using the two methods. Furthermore, due to the topographic characteristics of Taiwan, the concerned channel reaches for kinematic-wave routing (for example, from X_1 to X_3 in the Chung-Kang River as shown in Figure 2) are usually not affected by the tide (from the estuary to X_0 in Figure 2). Consequently, a normal-flow depth estimated from Manning's equation was used as the downstream boundary condition in the numerical experiments.

### Influences of slope and roughness on flood wave propagation

Figure 3 shows the triangular hydrographs used in the numerical experiments as upstream inflow conditions for different channel slopes. In these tests, the base time of the hydrograph was 20 h and the time to peak discharge was designed as 10 h. The channel length was 25 km and other parameters were set as $n = 0.02$, $B = 125$ m, and $Q_{IP} = 1,500$ m^3 s^{-1}. The deviation in the hydrographs using different flood-routing methods is significant for the case of $S = 0.0001$ and decreases as the channel slope increases. As shown in Figure 3(a), flood attenuation can be easily observed for both methods, and the dynamic-wave (DW) routing shows a more significant peak reduction in the outflow hydrograph than that for the kinematic-wave (KW) routing. This is because the kinematic-wave method has no explicit physical diffusion due to the omission of inertial and pressure forces, although the finite-difference solution induces numerical diffusion to reproduce an attenuation of the flood peak. Moreover, the omission of inertial forces and the component of pressure force reduces the propagation speed of the flood wave in the kinematic-wave routing, which causes a delay in the time to peak discharge compared with that observed in the dynamic-wave routing. Nevertheless, the deviation in the hydrographs using these two methods is almost imperceptible when the channel slope is equal to 0.001. As shown in Figure 3(d), the difference of peak discharge (DQ_p) between these two methods is only 0.0057 and the deviation of the time to peak discharge (DT_p) is zero in this test case.
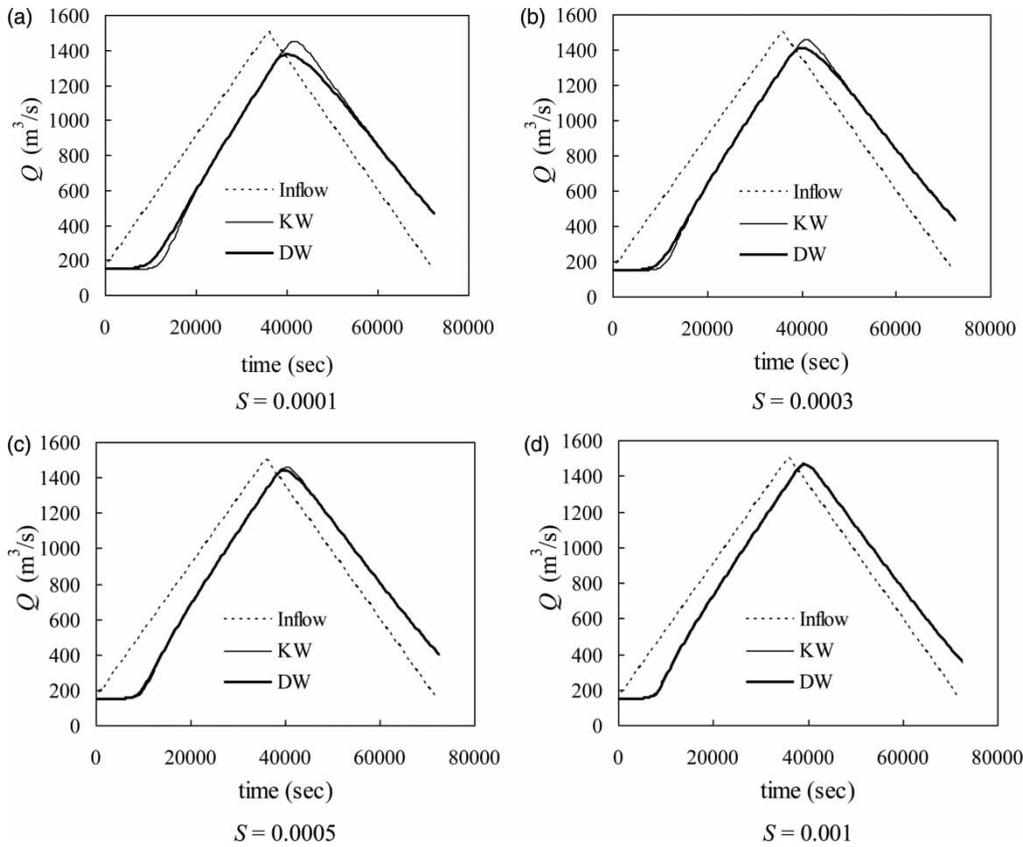
Figure 3 │ Comparison of hydrograph deviations by using dynamic- and kinematic-wave methods for different channel slopes ($B = 125$ m, $n = 0.02$, $L = 25$ km, $Q_{IP} = 1,500$ m^3 s^{-1}).

As shown in Figure 4, the hydrographs generated using the dynamic- and kinematic-wave algorithms were further grouped for convenient comparison to investigate the flood wave propagation in different channel-slope conditions. The figure demonstrates that the attenuation of the flood wave was generated by more physical and numerical diffusion in the dynamic-wave routing than that observed in the kinematic-wave routing. Moreover, the influences of channel roughness on hydrographs generated using the two methods are shown in Figure 5 for comparison.
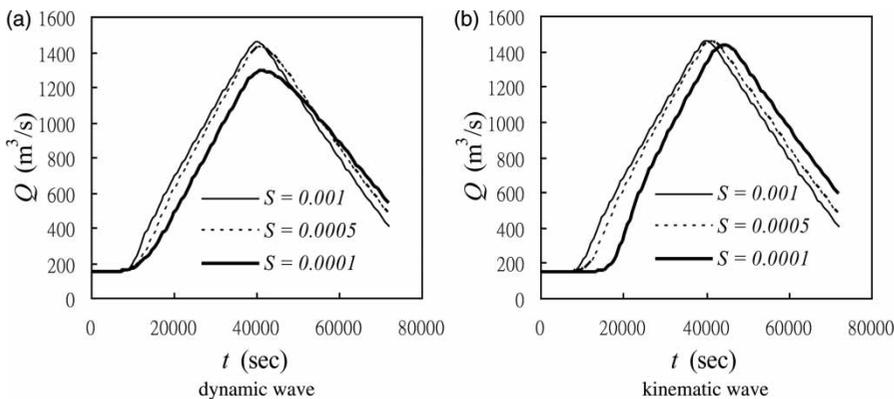
Figure 4 │ Hydrographs generated by using (a) dynamic- and (b) kinematic-wave methods for different channel slopes ($B = 125$ m, $n = 0.02$, $L = 25$ km).
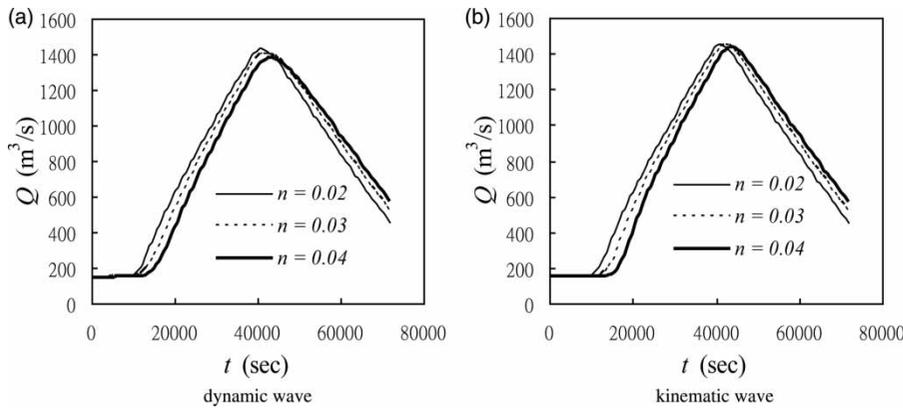
Figure 5 │ Hydrographs generated by using (a) dynamic- and (b) kinematic-wave methods for different channel roughnesses ($B = 125$ m, $S = 0.0005$, $L = 25$ km).

A delay in the hydrograph can clearly be observed in line with increasing channel roughness for both methods, and more attenuation of the peak discharge can be found using the dynamic-wave method in high channel roughness cases.

Influences of inflow hydrograph shape on flood wave propagation

As shown in Figures 3 and 4, the base time of the inflow hydrograph was set as 20 h in order to study peak unsteadiness in typhoon hydrographs of Taiwan. For comparison, different values of hydrograph base time were further performed to investigate the effect of hydrograph unsteadiness on the deviation in the hydrograph using these two methods. As shown in Table 1, a higher inflow unsteadiness results in a larger hydrograph deviation, especially for the peak-discharge deviation. For a channel slope larger than 0.001, even though the hydrograph duration is shortened to 10 h and the time to peak is shortened to 5 h, the peak discharge

deviation DQ_p is only 0.0014 and the time to peak discharge deviation DT_p is under 0.0009.

To investigate the influences of inflow hydrograph shape on flood wave propagation, a new set of inflow hydrograph following Pearson type-III distribution (Perumal & Sahoo 2008) was performed in the numerical tests for comparison. As shown in Figure 6, the peak discharge and time to peak discharge of the new hydrograph were set approximately to those in the original triangular inflow hydrograph. Figure 7 shows the comparison of outflow hydrograph deviations using the inflow hydrographs following Pearson type-III distribution. The numerical results in Table 2 reveal that the hydrograph deviation between these two methods in using the triangular inflow hydrograph is more obvious than that in using the Pearson type-III distribution hydrograph. It means that the criterion for ensuring the precision of the kinematic-wave approximation obtained in the numerical

Table 1 │ Hydrograph deviation between the dynamic- and kinematic-wave methods using different values of hydrograph base time

Base time of the inflow hydrograph (h)	Hydrograph deviation in the numerical experiments	
	DQ_P	DT_P
10	0.0014	0.0009
20	0.0007	0.0008
40	0.0004	0.0008

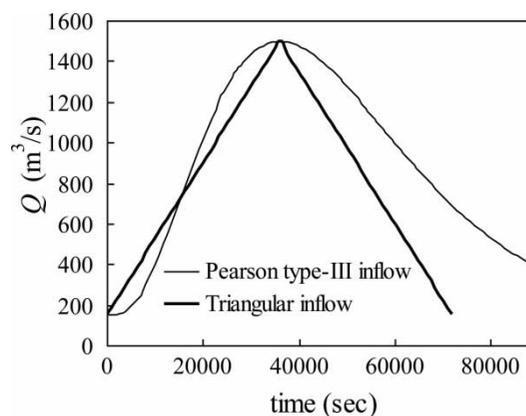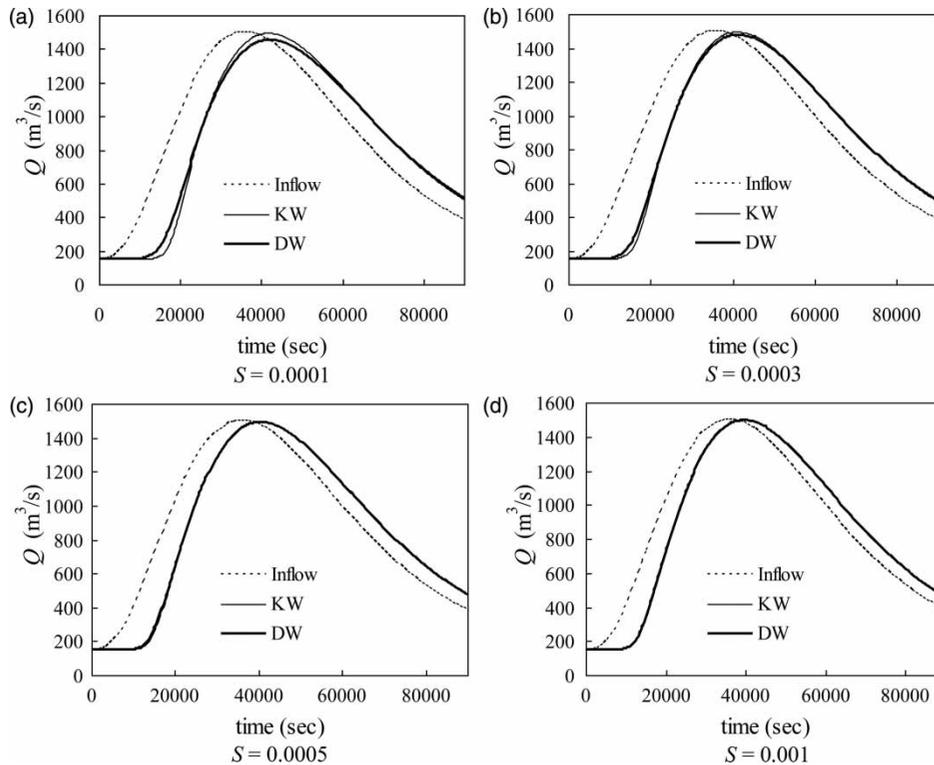*Note*: $S = 0.001$, $B = 125$ m, $n = 0.02$, $L = 25$ km, $Q_{IP} = 1,500$ m³ s⁻¹.

Figure 6 │ Inflow hydrograph following Pearson type-III distribution.

Figure 7 | Comparison of hydrograph deviations by using dynamic- and kinematic-wave methods for different channel slopes ($B = 125$ m, $n = 0.02$, $L = 25$ km, $Q_{IP} = 1,500$ m^3 s^{-1} and using a Pearson type-III distribution inflow hydrograph).

Table 2 | Hydrograph deviations between the dynamic- and kinematic-wave methods using different shapes of the inflow hydrograph

|	$S = 0.0001$		$S = 0.0003$		$S = 0.0005$		$S = 0.001$	
Inflow hydrograph	**DQ$_P$**	**DT$_P$**	**DQ$_P$**	**DT$_P$**	**DQ$_P$**	**DT$_P$**	**DQ$_P$**	**DT$_P$**
Triangle	0.076	0.052	0.035	0.022	0.016	0.008	0.0007	0.0008
Pearson type-III	0.043	0.007	0.013	0.007	0.004	0.006	0.0004	0.0001

Note: $B = 125$ m, $n = 0.02$, $L = 25$ km, $Q_{IP} = 1,500$ m^3 s^{-1}.

tests can be treated as a more stringent standard for further practical applications.

In fact, Figure 8 shows a typical flood hydrograph measured in the midstream of the Chung-Kang River. The steep topography and high rainfall intensity in Taiwan result in a short hydrological response time. The flood hydrograph looks like a triangular shape rather than a Pearson type-III distribution. Hence, the adoption of a triangular shape for the inflow hydrograph tests in this study should be considered reasonable to represent the geomorphologic and hydrological characteristics of Taiwan.

Integrated analysis for hydrograph deviations by using two methods

A series of numerical experiments were conducted to investigate the correlation between the four independent variables and the hydrograph deviations. In the numerical experiments, the range of the independent variables was channel slope $S = 0.0001$–0.005, channel roughness $n = 0.015$–0.05, channel width $B = 100$–300 m, and discharge in unit width $q = 5$–50 m^3 s^{-1}. More than 640 runs were performed in the course of the test. Since the kinematic-wave
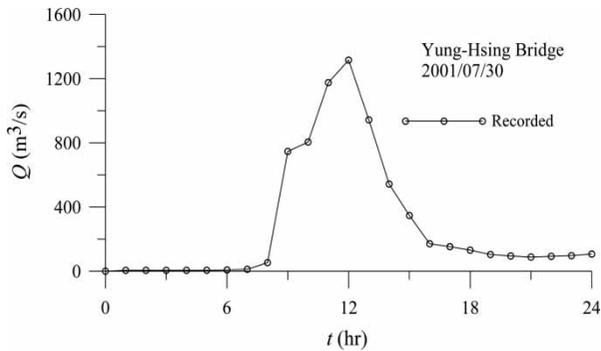
Figure 8 │ Flow record for a storm event occurred on July 30, 2001 at Yung-Hsing Bridge in the Chung-Kang River Basin.

approximation leads to a considerable simplification of the momentum equation, and is considered adequate for application only to channels with steep slope, concern should focus on the variation of hydrograph deviations with different channel slopes. As shown in Figure 9, the influences of the four independent variables on peak discharge deviation were evaluated. Different symbols are used in the figures for various channel-slope conditions to clarify the influences of slope and the other three independent variables on the deviation of peak discharge. In addition, Figure 3 demonstrates that a large hydrograph deviation can be observed in mild channels, and the scattering of the data points shown in Figure 9 further reveals three notable features. The first is that the grouping of the data points is mainly according to the variation of channel slope in spite of the changes in the other three variables. The second is that in considering the influences of the other three variables, the scatter range of the peak discharge deviation for a steep channel is smaller compared with that for a mild channel. Moreover, a value of DQ_p larger than 0.07 can only result from a channel slope smaller than 0.0005, and a deviation smaller than 0.025 can only occur in the case of a channel slope larger than 0.001. An evaluation of the influences of the independent variables on the time to peak discharge deviation (DT_p) was conducted, and the results are shown in Figure 10. Basically, the same tendency for the scattering of data points can be observed in both Figures 9 and 10. Therefore, the first two notable features of Figure 9 described above are also applicable to the data points shown in Figure 10.

A regression analysis was further provided to examine the interrelation between the hydrograph deviations and the four independent variables in this study. A Tobit regression method was adopted to create a more realistic model for left-censored dependent variables. For a test channel length of 25 km, the regression results for the peak discharge deviation and time to peak-discharge deviation are:

$$DQ_p = 5.123 \times 10^{-5} S^{-2.129} n^{2.449} \left(\frac{B}{y_{IP}} \right)^{-0.102} \left(\frac{Q_{IP}}{B y_{IP}^{1.5} g^{0.5}} \right)^{1.256}$$

(16)

$$DT_p = 1.083 \times 10^{-4} S^{-1.850} n^{2.163} \left(\frac{B}{y_{IP}} \right)^{0.003} \left(\frac{Q_{IP}}{B y_{IP}^{1.5} g^{0.5}} \right)^{1.665}$$

(17)

In performing the regression analysis, a significant level is usually used to evaluate the degree of influence of the independent variables on the dependent variables. An independent variable can be recognized as a dominant term to the dependent variable if the value of the significant level is less than 0.1. Based on the Tobit regression analysis, the values of the significant level for the last two independent variables shown in Equations (16) and (17) are larger than 0.1; they are less than 0.1 for channel roughness n and less than 0.01 for the channel slope S. It can therefore be concluded that channel slope has the most significant influence on the hydrograph deviations, while channel roughness also plays an important role in affecting the deviation of the outflow hydrographs, which has been shown explicitly in Figures 9 and 10.

Although the Tobit regression analysis has revealed the dominance of channel slope on the hydrograph deviations compared to the other three independent variables, the amount of hydrograph deviation should increase as the channel length increases. Consequently, as shown in Figure 11, numerical tests with an experimental channel length of 50 km were added to compare with the results from the 25 km channel as shown in Figure 3. For a channel length of 25 km, the deviation of peak discharge between
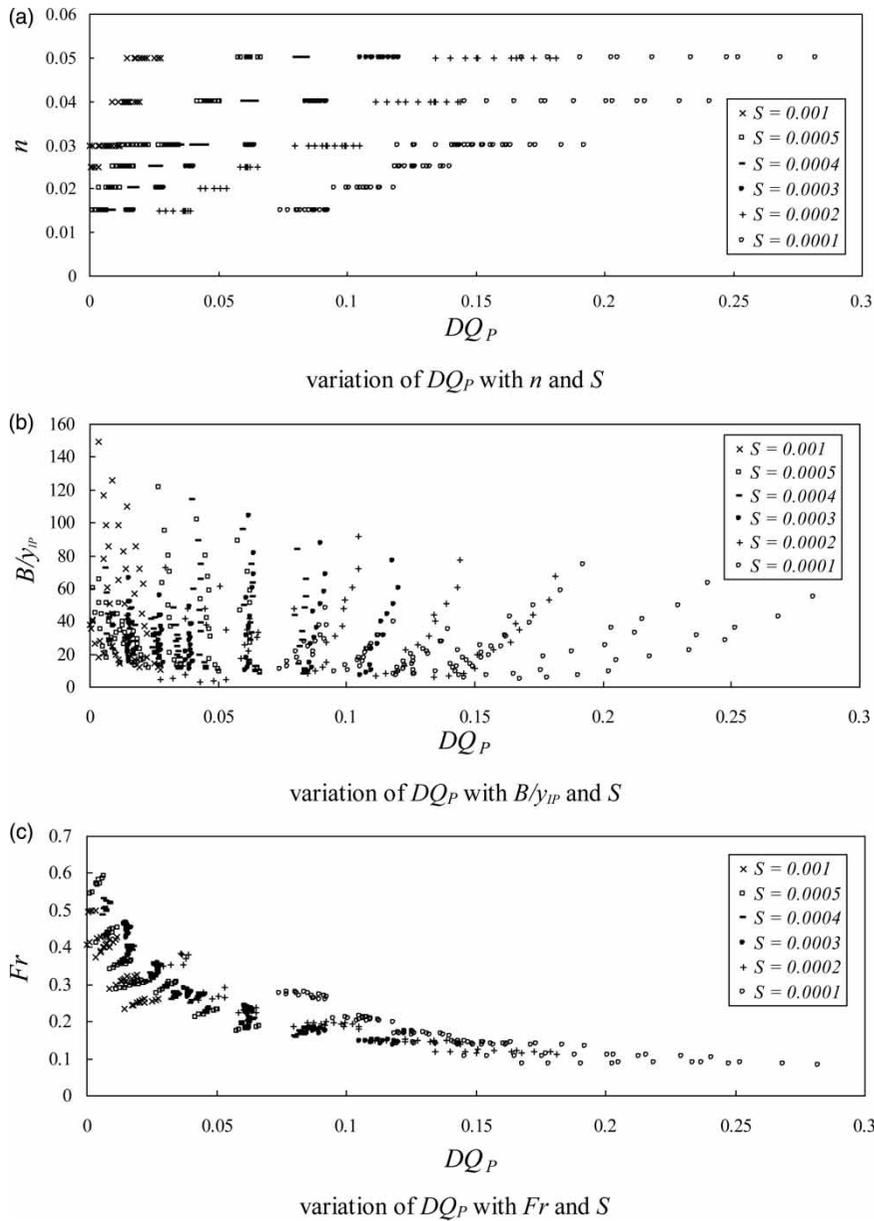
Figure 9 | Variation of peak discharge deviation with independent variables.

the dynamic- and kinematic-wave methods is 0.074 for a channel slope of 0.0001 (Figure 3(a)), and is 0.0057 for a channel slope of 0.001 (Figure 3(d)). When routing the inflow hydrograph in a channel of 50 km, although the peak discharge deviation reaches 0.0162 for a channel slope of 0.0001 (Figure 11(a)), it is only 0.0098 for a channel slope of 0.001 (Figure 11(b)), which is almost imperceptible. The results demonstrate that the hydrograph deviation between these two flood-routing methods is negligible for

a channel slope larger than 0.001, even if the flood-wave routing is performed in a channel 50 km long.

CONCLUSIONS

The deviation of hydrographs between the kinematic- and dynamic-wave methods arises from the omission of inertial forces and the component of the pressure force in the
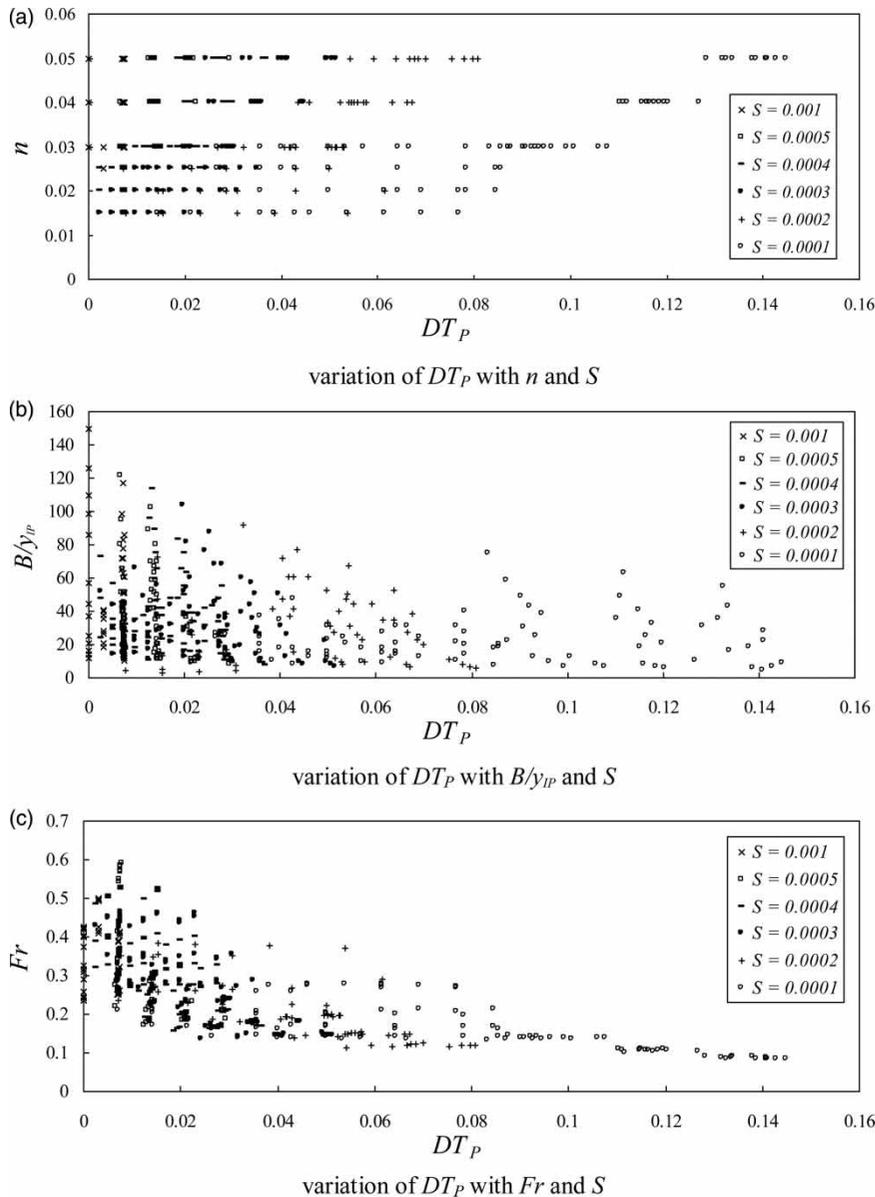
(a) variation of DT_P with n and S

(b) variation of DT_P with B/y_{IP} and S

(c) variation of DT_P with Fr and S

Figure 10 │ Variation of time to peak discharge deviation with independent variables.

kinematic-wave approximation. The omission of these two terms decreases the propagation speed of the flood wave and also reduces flood peak attenuation. In this study, hydrograph deviations between these two routing methods were evaluated quantitatively on the basis of peak discharge and time to peak discharge using two dimensionless parameters. The numerical tests were performed in a rectangular channel using triangular hydrograph as the upstream inflow boundary conditions. The results of the

numerical simulation reveal that channel slope dominates the deviation of the hydrographs. Nevertheless, the peak discharge deviation DQ_p is within 0.025 and the time to peak discharge deviation DT_p is within 0.007 for a channel slope larger than 0.001 in a channel length of 50 km. Since the slopes of the channel reaches in Taiwan to which the kinematic-wave approximation applies are usually larger than 0.001 and the channel lengths are shorter than 50 km, it is considered acceptable to employ the
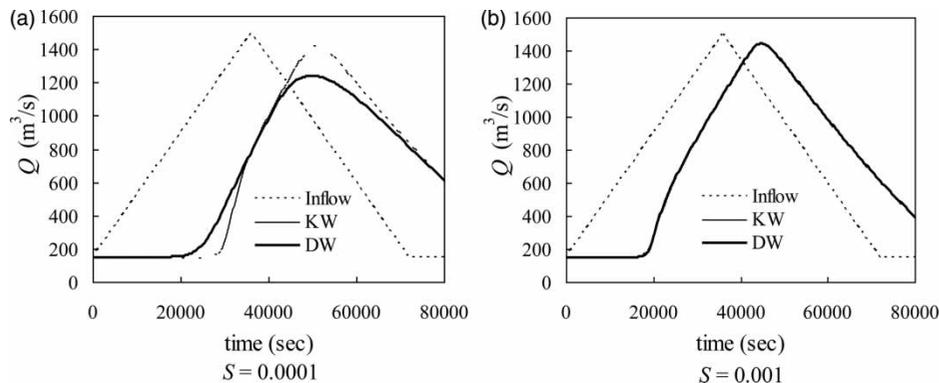
Figure 11 | Comparison of hydrograph attenuation in channels with different slopes by using dynamic- and kinematic-wave methods ($B = 125$ m, $n = 0.02$, $L = 50$ km).

kinematic-wave method in developing a real-time flood forecasting system, using the dynamic-wave routing in the downstream tidal reaches and the kinematic-wave approximation in the upper channel reaches whose slopes are larger than 0.001. This effectively alleviates the numerical instability problems induced by transcritical flow conditions.

ACKNOWLEDGEMENTS

REFERENCES

Abbott, M. A. 1976 Computational hydraulics: a short pathology. *J. Hydraul. Res.* **14**, 271–285.

Akan, A. O. & Yen, B. C. 1981 Diffusion-wave flood routing in channel networks. *J. Hydraul. Div. ASCE* **107**, 719–732.

Cappelaere, B. 1997 Accurate diffusive wave routing. *J. Hydraul. Eng. ASCE* **123**, 174–181.

Chow, V. T., Maidment, D. R. & Mays, L. W. 1988 *Applied Hydrology.* McGraw-Hill, New York, USA, pp. 294–296.

Courant, R., Friedrichs, K. & Lewy, H. 1967 On the partial difference equations of mathematical physics. *IBM Journal* **11**, 215–34.

Cundy, T. W. & Tento, S. W. 1985 Solution to the kinematic wave approach to overland flow routing with rainfall excess given by the Philip equation. *Water. Resour. Res.* **21**, 1132–1140.

Cunge, J. A. 1969 On the subject of a flood propagation method. *J. Hydraul. Res.* **7**, 205–230.

Cunge, J. A., Holly, F. M. & Verwey, A. 1980 *Practical aspects of computational river hydraulics.* Pitman, London, pp. 132–184.

Fread, D. L. 1973 Technique for implicit dynamic routing in rivers with major tributaries. *Water Resour. Res.* **9**, 918–926.

Fread, D. L. 1985 Channel routing. Ch. 14 in *Hydrological Forecasting* (M. G. Anderson & T. P. Burt, eds.) John Wiley & Sons, Inc., New York, N.Y., pp. 437–503.

Henderson, F. M. & Wooding, R. A. 1964 Overland flow and groundwater flow from a steady rainfall of finite duration. *J. Geophys. Res.* **69**, 1531–1540.

Huang, J.-K. & Lee, K. T. 2009 Influences of spatially heterogeneous roughness on flow hydrographs. *Adv. Water Resour.* **32**, 1580–1587.

Iwagaki, Y. 1955 Fundamental Studies on Runoff Analysis by Characteristics. Bulletin 10, Disaster Prevention Research Institute, Kyoto University, pp. 1–25.

Jaber, F. H. & Mohtar, R. H. 2003 Stability and accuracy of two-dimensional kinematic wave overland flow modeling. *Adv. Water Resour.* **26**, 1189–1198.

Jin, M. & Fread, D. L. 1997 Dynamic flood routing with explicit and implicit numerical solution schemes. *J. Hydraul. Eng. ASCE* **123**, 166–173.

Lee, K.T. & Yen, B.C. 1997 Geomorphology and kinematic-wave based hydrograph derivation. *J. Hydraulic. Eng. ASCE* **123**, 73–80.

Lighthill, M. J. & Whitham, G. B. 1955 On kinematic waves, I. Flood movement in long rivers. *Proc. Ser. A: Math. Phys. Sci. Roy. Soc. London* **229**, 281–316.

Meselhe, E. A. & Holly Jr, F. M. 1997 Invalidity of Preissmann scheme for transcritical flow. *J. Hydraul. Eng. ASCE* **123**, 652–655.

Perumal, M. & Sahoo, B. 2008 Volume conservation controversy of the variable parameter Muskingum–Cunge Method. *J. Hydraulic Eng. ASCE* **134**, 475–485.

Ponce, V. M. 1991 Kinematic wave controversy. *J. Hydraul. Eng. ASCE* **117**, 511–525.

Ponce, V. M. & Yevjevich, V. 1978 Muskingum-Cunge method with variable parameters. *J. Hydraul. Div. ASCE* **104**, 1663–1667.

Ponce, V. M., Li, R. M. & Simmons, D. B. 1978 Applicability of kinematic and diffusion models. *J. Hydraul. Div.* ASCE **104**, 353–360.

Preissmann, A. 1961 *Propagation des intumescences dans les canaux et rivieres*. 1re Congr. des l'Assoc. Francaise de Calcul, Association Francaise de Calcul, Grenoble, France, pp. 433–442. (In French)

Price, R. K. 1973 Variable parameter diffusion method for flood routing. Report No. INT 115, Hydraulic Research Station, Wallingford, U.K.

Price, R. K. 1974 A comparison of four numerical methods for flood routing, *J. Hydraul. Div. ASCE* **100** (HY7), 879–899.

Price, R. K. 2009 Volume-conservative non-linear flood routing. *J. Hydraul. Eng. ASCE* **135**, 838–845.

Samuels, P. G. & Skeels, C. P. 1990 Stability limits for Preissmann's scheme. *J. Hydraul. Eng. ASCE* **116**, 997–1012.

Tang, X., Knight, D. W. & Samuels, P. G. 1999 Volume conservation in variable parameter Muskingum-Cunge method. *J. Hydraul. Eng. ASCE* **125**, 610–620.

Todini, E. 2007 A mass conservative and water storage consistent variable parameter Muskingum-Cunge approach. *Hydrol. Earth Syst. Sci.* **4**, 1549–1592.

Tseng, M-H. 2010 Kinematic wave computation using an efficient implicit method. *J. Hydroinformatics* **11**, 329–338.

Wooding, R. A. 1965 A hydraulic model for the catchment-stream problem. *J. Hydrol.* **3**, 254–267.

Yen, B. C. & Tsai, C. W.-S. 2001 On non-inertia wave versus diffusion wave in flood routing. *J. Hydrol.* **244**, 97–104.

Ying, X., Khan, A. A. & Wang, S. S. Y. 2004 Upwind conservative scheme for the Saint Venant equations. *J. Hydraul. Eng. ASCE* **130**, 977–987.